

# Brownian dynamics of concentrated polymers in two dimensions<sup>1</sup>

G. Ianniruberto <sup>a,\*</sup>, G. Marrucci <sup>a</sup>, E.J. Hinch <sup>b</sup>

<sup>a</sup> *Dipartimento di Ingegneria Chimica, Università di Napoli, Piazzale Tecchio, 80125 Napoli, Italia*

<sup>b</sup> *Department of Applied Mathematics and Theoretical Physics, University of Cambridge, Silver Street, Cambridge CB3 9EW, UK*

Received 31 July 1997

---

## Abstract

Two-dimensional simulations of the Brownian dynamics of polymers in a grid of topological obstacles were carried out in this study. A first model made use of the exact expression for the free energy of a chain with fixed ends interacting with an obstacle and can be used to derive the elastic force acting on the subchains of a Rouse-like model. With this model we calculated the diffusion coefficient of chains of different lengths constrained by the fixed obstacles. A second model, less rigorous but more efficient computationally, was used to simulate the chain dynamics in fast flows. In such a case, the obstacles were convected according to the shear gradient. During the simulation, the configurational changes of the chain constrained by the obstacles could be monitored and the stresses which developed were calculated. These simulations reveal important effects of the conformational fluctuations at high shear rates. © 1998 Elsevier Science B.V. All rights reserved.

*Keywords:* Brownian dynamics; Concentrated polymeric liquids; Two-dimensional dynamics; Topological obstacles; Fast flows

---

## 1. Introduction

The dynamics of concentrated polymeric liquids is very complex and far from being completely understood. Polymer–polymer interactions known as entanglements become important above critical values of molecular weight and concentration. In the case of melts, the observed behaviour for  $M > M_c$  departs dramatically from predictions based merely on frictional interactions, i.e. from the predictions of the Rouse model [1].

---

\* Corresponding author. Fax: + 39 81 2391800.

<sup>1</sup> Dedicated to the memory of Professor Gianni Astarita.

The many-body problem of concentrated polymers was ingeniously reduced to a single-body one by proposing that chains can be considered as being effectively confined to a tube-like region [2]. The equilibrium dynamics of entangled polymers was then described by the reptation model [3], whereby chains can move long distances only by slithering along the tube.

Rheological properties of entangled polymers are reasonably described by the tube model of Doi and Edwards [4], especially in the linear limit of slow flows. In the non-linear range however, the standard tube model is not equally satisfactory. In particular, in shear flows the steady-state shear stress is predicted to go through a maximum with increasing shear rate above the linear range, a feature which implies an instability. However, experiments usually show a wide region of shear rates above the linear range where the shear stress remains an increasing function of shear rate with no sign of instability. This disagreement indicates that something is missing in the basic theory, which becomes important in fast flows.

In strong shear flows, reptation is effectively suppressed and tubes tend to align to the flow direction. Lateral fluctuations of the chain as measured by the tube diameter can then become important. Some recent papers [5,6] considered such effects, but no definitive conclusion could be reached. In particular, Spensley and Cates [6] modelled the chain both as a dumbbell and as a Rouse chain constrained in the aligned tube. Surprisingly, they found out that the stress predictions were strongly model dependent, although, without the tube, it is well known that the dumbbell and the Rouse model are essentially equivalent in steady shear.

In this paper, we report on some numerical simulations of Brownian dynamics in two dimensions which are related to the problem outlined above. We consider a chain constrained in an infinite grid of obstacles (the crosses in Fig. 1), regularly spaced for numerical convenience. We further assume that at equilibrium the obstacles are fixed whereas under flow conditions they move affinely. We first consider an approach where the dynamics is based on the rigorous formula for the free energy of a chain interacting with an obstacle, independently derived by Edwards [7] and by Saito and Chen [8] long ago, yet never used in simulations of entangled chain dynamics. Some interesting results for the diffusion coefficient of the chain were obtained in this way. For the fast flow problem however, a different model was adopted for which the obstacle uncrossability condition is enforced through simpler expressions of the interaction potential. It was then possible to obtain stress predictions in fast flows.

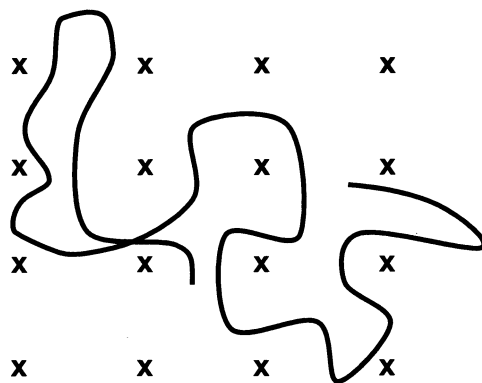


Fig. 1. Two-dimensional picture of an entangled chain.

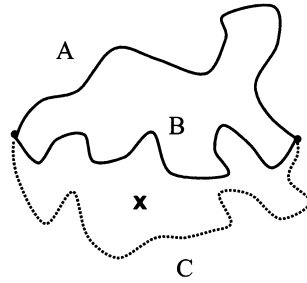


Fig. 2. A chain with fixed ends interacting with an obstacle (cross). Configurations such as the dotted one are forbidden.

## 2. Chain dynamics under quiescent conditions

Let us start by considering the interaction of a chain with a single obstacle. With reference to Fig. 2, consider temporarily that the chain ends are frozen. Then, if A is the initial configuration of the chain, configurations of the B type can be explored whereas those of the C type are forbidden by the obstacle. Since the topological interaction reduces the number of possible configurations, it modifies the free energy of the polymer. Let  $\mathbf{R}_1$  and  $\mathbf{R}_2$  be the position vectors of the chain ends measured from the obstacle O (cf Fig. 3) and let  $\alpha$  be the angle spanned by the position vector in moving along the chain from one end to the other ( $\alpha > 2\pi$  in the example of Fig. 3). Note that the chain is not ‘entangled’ when  $\alpha < \pi$ . The three scalars  $R_1$ ,  $R_2$  and  $\alpha$  are the state variables of the chain (in two dimensions). Edwards [7] and Saito and Chen [8] demonstrated that the free energy  $A$  of the chain is given by

$$A(R_1, R_2, \alpha) = kT \left[ \frac{R^2}{R_0^2} + z \cos \alpha - \ln \left( 2 \int_0^\infty I_\nu(z) \cos(\alpha\nu) d\nu \right) \right], \quad (1)$$

where  $R^2 = (\mathbf{R}_2 - \mathbf{R}_1)^2$  is the end-to-end square distance and  $R_0^2$  is the average value for such a quantity when the chain is free. Chain ‘distance’ from the obstacle is measured by  $z = 2R_1R_2/R_0^2$ , while  $I_\nu$  indicates the modified Bessel function. The first term in Eq. (1) is the classical Gaussian contribution for ideal chains in the free state, while the other two terms account for the topological interaction in a rigorous way. They make the free energy a complicated function of the state variables.

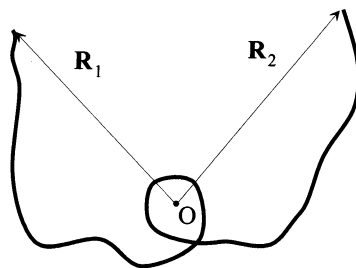


Fig. 3. A chain going around an obstacle placed at the origin. The relevant coordinates are  $R_1$ ,  $R_2$ ; and the angle  $\alpha$  (not shown). The latter is spanned by the position vector when moving along the chain from one end to the other.

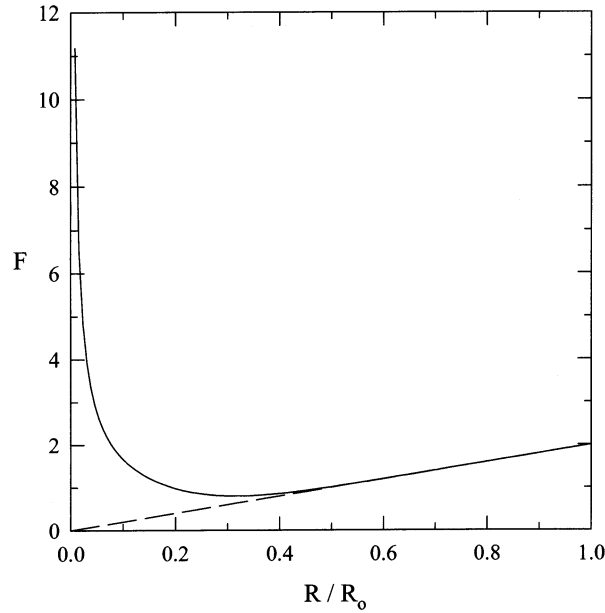


Fig. 4. The entropic force (in units of  $k_B T / R_0$ ) vs. the end-to-end distance  $R / R_0$  for a chain having  $R_1 = R_2$  (see Fig. 3) and  $\alpha = \pi/4$ .

From the free energy we can compute the entropic forces acting on the chain ends (in the chain ends we will concentrate friction as in the classical dumbbell model). By using the principle of virtual works we write

$$\mathbf{F}_i = -\frac{\partial A}{\partial \mathbf{R}_i} \frac{\mathbf{R}_i}{R_i} - \frac{1}{R_i} \frac{\partial A}{\partial \alpha} \mathbf{n}_i \quad i = 1, 2, \quad (2)$$

where  $\mathbf{n}_i$  is the unit vector normal to  $\mathbf{R}_i$  in the direction of increasing  $\alpha$ . Eqs. (1) and (2) show that the elasticity of the chain becomes strongly non-linear because of the obstacle.

As an example, Fig. 4 reports the modulus  $F$  of the entropic force as a function of the end-to-end distance in the non-entangled symmetric case  $R_1 = R_2$  (and for a fixed angle  $\alpha = \pi/4$ ). Fig. 5 shows the corresponding orientation  $\phi$  of the entropic force with respect to the end-to-end direction. In the limit of zero chain-obstacle distance, the force diverges (cf. Fig. 4), i.e. the obstacle strongly repels the chain. Figs. 4 and 5 also show that for the ‘free’ chain ( $\alpha < \pi$ ) the force recovers the classical proportionality with the end-to-end vector when the bead-obstacle distance becomes of the order of  $R_0$ , i.e. the topological effect becomes negligible over distances of the order of the chain equilibrium size. In the entangled case ( $\alpha > \pi$ ), since  $\partial A / \partial \alpha$  is a positive quantity, the entropic force works in the direction of disentangling the chain.

As previously mentioned, the free energy (hence the force) is a function of three variables. However, Eq. (1) shows that the complicated part of the expression, namely the topological contribution, is a function of only two variables, namely  $z$  and  $\alpha$ . For numerical convenience, we have chosen to create once and for all a table of values for each of the derivatives  $\partial A / \partial z$  and  $\partial A / \partial \alpha$  entering the force expression. Thus, when a value of these derivatives is required for given

$z$  and  $\alpha$ , a linear interpolation of the stored values can readily be performed. The tables extend up to values of  $z$  and  $\alpha$  beyond which simpler asymptotic expressions apply ( $z > 5$  and  $\alpha > 8\pi$ ).

### 2.1. Diffusion of a dumbbell in the grid of obstacles

The simplest case to be considered is when the chain size is so small with respect to the mesh size of the grid of obstacles that at any time, the chain only feels the topological effect of, at most, one of them. Hence, by modeling the chain as a dumbbell, Eq. (1) applies and the elastic force acting on the end beads is given by Eq. (2). The diffusion of a dumbbell is then studied by Brownian dynamics, i.e. through numerical integration of the Langevin equations for the end beads:

$$\zeta \frac{d\mathbf{R}_i}{dt} = \mathbf{F}_i + \mathbf{f}_i \quad i = 1, 2. \quad (3)$$

Here,  $\zeta$  is the bead friction coefficient with the background material, i.e. with the solvent in the case of solutions or with the bulk polymer in the case of melts. However,  $\zeta$  is independent of topology as the latter is explicitly considered in the simulation. In Eq. (3),  $\mathbf{R}$  is the position vector measured from the closest obstacle and  $\mathbf{f}$  is the Brownian force obeying

$$\langle \mathbf{f}_i \rangle = 0; \quad \langle \mathbf{f}_i(t) \mathbf{f}_j(t + \tau) \rangle = 2\zeta k_B T \delta(\tau) \delta_{ij} \mathbf{1} \quad (4)$$

The symbol  $\langle \dots \rangle$  indicates ensemble averaging,  $\delta$  is the Dirac delta function,  $\delta_{ij}$  is the Kronecker delta and  $\mathbf{1}$  is the unit tensor.

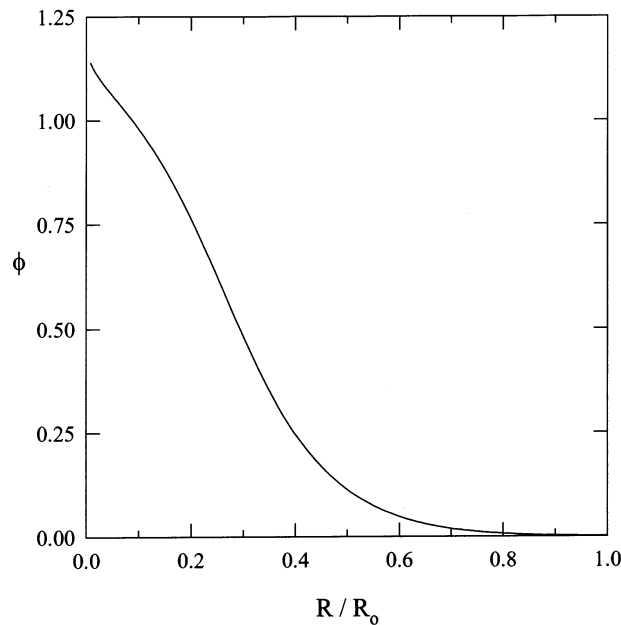


Fig. 5. The angle  $\phi$  by which the entropic force is ‘off’ with respect to the end-to-end direction for the same chain of Fig. 4. This angle vanishes when  $R \cong R_0$ .

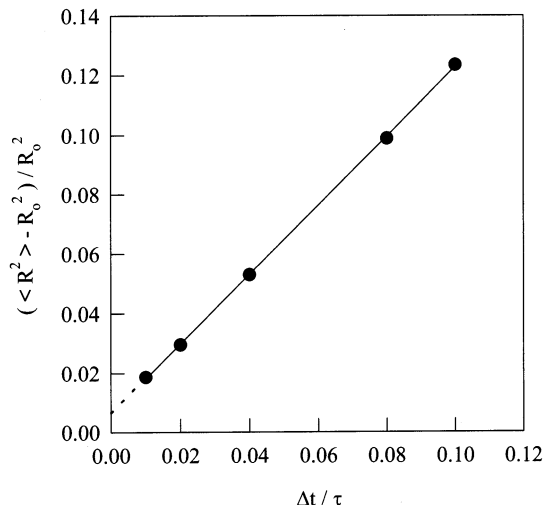


Fig. 6. Deviation of the mean square end-to-end distance of the chain in the grid of obstacles vs. the time step  $\Delta t$  used in the simulation.

Although Eq. (3) accounts for the chain-obstacle topological interaction through the entropic force  $F$ , the equation only describes bead trajectories. The ‘non-phantom’ character of the chain between the beads must be accounted for separately by checking that no improper crossing of the obstacles takes place. Thus, in carrying out the integration in time of Eq. (3), the possible change of topology must be checked at each time step. Such a change occurs whenever the angle  $\alpha$  crosses integer multiples of  $\pi$  (cf. Fig. 3). Checking the topology at each time step, although geometrically simple, is one of the time consuming aspects of this procedure.

With regard to details and difficulties related to Brownian dynamics simulations in general, reference is made to recent textbooks [9,10]. In particular, it is well known that the numerical integration of the Langevin equation is sensitive to the time step  $\Delta t$ . However, extrapolation of the results obtained at several  $\Delta t$  values to  $\Delta t = 0$  solves this problem. We used a Euler method and averages were obtained over a population of 25 000 molecules. As usual, the simulations were made in nondimensional variables: the mesh size  $a$  of the obstacle grid is our unit of length and  $\tau = \zeta R_0^2 / 2k_B T$  is the unit time.

The quality of the simulation is shown in Figs. 6 and 7. Fig. 6 reports the deviation of the average square size of the dumbbell in the grid of obstacles with respect to the free-chain value. Such a deviation should be zero, as purely topological obstacles (with no excluded volume) do not alter equilibrium properties but only dynamical ones. Indeed, as shown in Fig. 6, the value of the deviation extrapolated to  $\Delta t = 0$  is less than 1%, which was deemed acceptable (remember that the elastic force is calculated from Eq. (2) with some inevitable approximation). Fig. 7 shows that the correlation decays exponentially. It also shows that the relaxation time of the chain in the grid of obstacles is indistinguishable from that of the free chain, the difference being less than 1%, well within the calculation accuracy.

A dynamical property which proves to be sensitive to the obstacles is the center-of-mass diffusivity. Fig. 8 shows a diffusivity reduction (extrapolated to  $\Delta t = 0$ ) of about 4% for a ‘small’

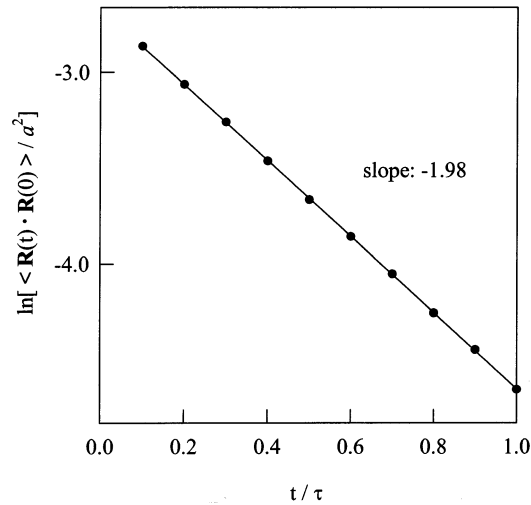


Fig. 7. Decay in time of the end-to-end correlation for the dumbbell between the obstacles. With the units used, the slope for the free chain is  $-2$ .

chain ( $R_0 = 0.25a$ ), while Fig. 9 emphasises the dependence on size. It is clear that larger chains bump into the obstacles more frequently than smaller ones, thus reducing their diffusivity.

## 2.2. Diffusion of a Rouse chain in the grid of obstacles

The diagram in Fig. 9 could not be continued to larger chains because interactions of the dumbbell with more than one obstacle at a time would have occurred, a situation which is not

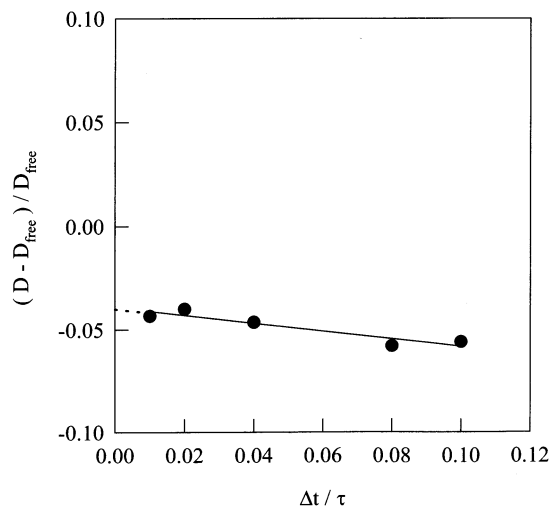


Fig. 8. The diffusivity of a chain having a size  $R_0 = 0.25a$  ( $a$  is the mesh size of the obstacle grid) is found to be 4% less than that of a free chain.

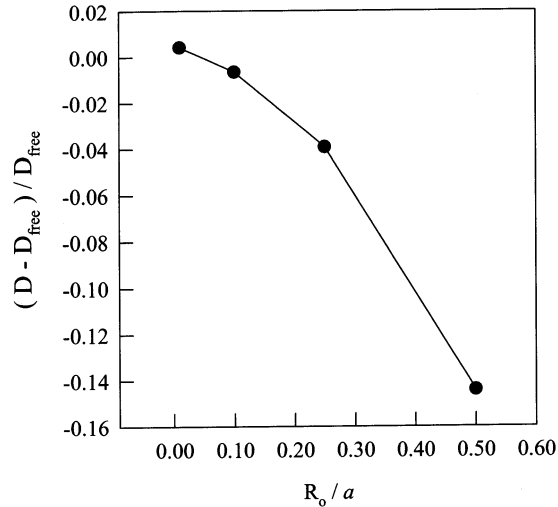


Fig. 9. Relative drop in diffusivity with increasing  $R_0/a$  for the dumbbell model.

directly compatible with the free-energy formula in Eq. (1). Larger chains can nevertheless be considered if they are divided in subchains. Thus, although the chain interacts with many obstacles at a time, each subchain interacts with one of them at most and the basic formula for the elastic force, Eq. (2), can still be applied to the subchains. In other words, longer chains must be modeled as Rouse chains whose beads obey a Langevin equation like Eq. (3) (where the elastic force is the sum of two terms for all internal beads).

Fig. 10 reports the mean square end-to-end distance of the Rouse chain as a function of the number  $N$  of subchains, the equilibrium length of the subchains being fixed at the value  $b = 0.25a$ . The averages are made over 8000 molecules and the time step is chosen once and for all equal to  $0.01\tau$ , where  $\tau = \zeta b^2/2k_B T$  is (one half) the relaxation time of the subchain. Here again we find that the mean square end-to-end distance is not affected by the obstacles (to better than 1%). The slope in Fig. 10 is consistent with the chosen  $b$  value.

The results for the center-of-mass diffusivity are reported in Fig. 11. As one would expect, the reduction in diffusivity grows with chain size. What is perhaps unexpected is the ‘length’ of the transition to the entangled state; the data show a slope of  $-1.3$  over almost a decade. Since the ultimate slope of the fully entangled state is  $-2$ , such a state is still far away in chain-length space, even for the longest chain considered in these simulations. Yet the diffusivity is already considerably reduced. However, self-consistency would perhaps require that also the obstacle density should increase by increasing chain length. In such a case, the transition to the entangled state would occur more rapidly.

That topology can introduce ‘strange’ power laws is indicated by the results in Fig. 12, which refer to the case  $N = 3$ . Here the relaxation of the end-to-end correlation for the entangled chain is compared with the corresponding relaxation in the dilute case. The correlation function in the concentrated case does not decay as a simple exponential, but rather as a ‘stretched’ exponential. A similar dynamic behaviour was recently observed by Shaffer [11] in Monte Carlo simulations of concentrated systems on a 3D lattice.

Although the simulation technique described thus far seems generally satisfactory, the computing time soon becomes too large with increasing  $N$ . One reason is that the topology check referred to in the previous section must be applied at each time step to each subchain. However, since the sub-chain length must remain well below the obstacle mesh size, highly entangled chains require large  $N$  values. A second reason applies to Rouse chain simulations in general, i.e. that the time step must be made small with respect to the relaxation time of the sub-chain, rather than of the chain as a whole. In conclusion, this technique proves too expensive if fast flows of longer chains are to be simulated.

### 3. High shear rate dynamics

In the model adopted in this section, the non-crossing condition between the chain and the obstacles is obtained more simply by giving the obstacles a non-zero size and by making the subchains stiff Fraenkel springs. In this case therefore, together with the topological effect, excluded volume interactions also come into play.

The hard core potential representative of the obstacle size was in fact smoothed (for numerical convenience) by introducing a repulsive force  $\mathfrak{F}$  whose magnitude has the form

$$\mathfrak{F}(d) = M \{1 - \tanh[q(d - s)]\}, \quad (5)$$

where  $M$ , the maximum force intensity, is sufficiently large with respect to elastic and Brownian forces to enforce the topological constraint. Its precise value is otherwise irrelevant. In Eq. (5),  $s$  is the obstacle size,  $d$  is the obstacle-bead distance and  $q$  is the reciprocal length over which the repulsive force jumps from zero to  $M$ .

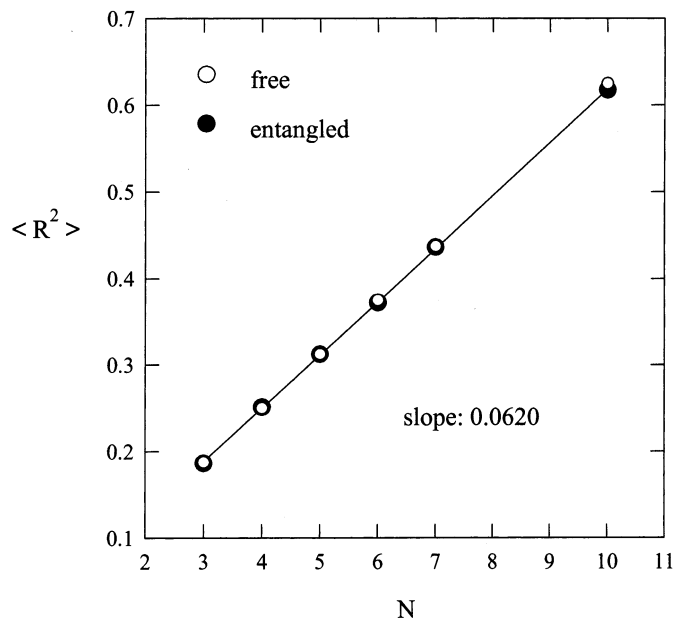


Fig. 10. Mean square end-to-end distance of free and entangled Rouse chains vs. the number  $N$  of sub-chains.

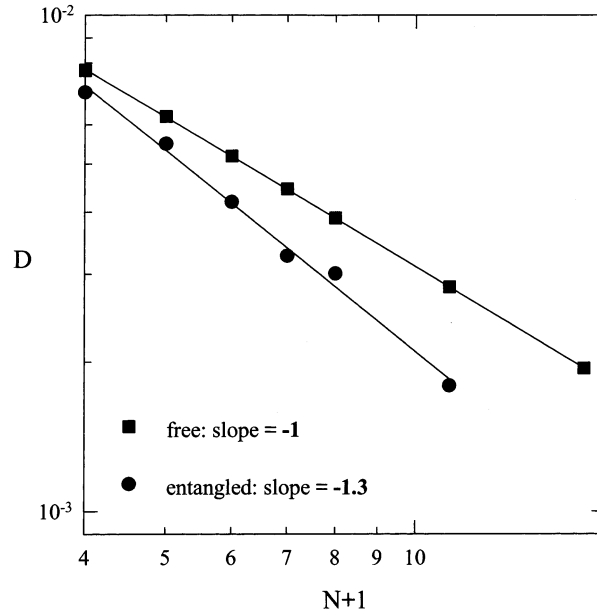


Fig. 11. Diffusivity of free and entangled Rouse chains vs. the number of beads. The results for the entangled chains are fitted with a  $-1.3$  power law.

The magnitude of the elastic force  $F$  of the Fraenkel dumbbell is given by [12]

$$F(\ell) = K(\ell - \ell_0), \quad (6)$$

where  $K$  is the elastic constant,  $\ell$  is the current spring length and  $\ell_0$  its ‘natural’ value. To enforce the uncrossability condition,  $\ell_0$  must be smaller than  $2s$  and  $K$  large. Here again, precise values of these parameters are essentially irrelevant.

For entangled multiple bead-spring chains in shear flow, the Langevin equation for the beads then takes the form

$$\zeta \left( \frac{d\mathbf{R}_i}{dt} - \dot{\gamma} \mathbf{R}_i \cdot \mathbf{e}_y \mathbf{e}_x \right) = \mathbf{F}_{i+1} - \mathbf{F}_i + \mathbf{f}_i + \mathfrak{S}_i \quad i = 0, \dots, N, \quad (7)$$

where  $\mathbf{R}_i$  is now the position vector of the generic bead with respect to a fixed frame of reference,  $\dot{\gamma}$  is the shear rate,  $\mathbf{e}_x$  is the unit vector in the shear direction and  $\mathbf{e}_y$  that in the gradient direction. In Eq. (7), the  $i$ th elastic force  $\mathbf{F}_i$  is due to the Fraenkel spring between beads  $i-1$  and  $i$ . For the end beads,  $\mathbf{F}_0 = \mathbf{F}_{N+1} = 0$ .

In relation to a flow problem, the most interesting factor observable is the stress tensor. In our case, the polymer stress  $\mathbf{T}$  is made up not only of the classical Brownian and elastic terms, but also of the repulsive contribution due to bead-obstacle interaction. The overall expression for  $\mathbf{T}$  is given by

$$\mathbf{T} = v \left\langle \sum_{i=0}^N [\mathbf{R}_i (\mathbf{f}_i + \mathbf{F}_{i+1} - \mathbf{F}_i) + (\mathbf{R}_i - \mathbf{O}_i) \mathfrak{S}_i] \right\rangle, \quad (8)$$

where  $\nu$  is the number of chains per unit volume and  $\mathbf{O}_i$  is the position vector of the obstacle closest to bead  $i$  at time  $t$ . The obstacles are simply convected by the flow, i.e. the change in time of  $\mathbf{O}_i$  obeys:  $d\mathbf{O}_i/dt = \dot{\gamma}\mathbf{O}_i \cdot \mathbf{e}_y \mathbf{e}_x$ . The first term on the right hand side of Eq. (8) is the classical Kramer's expression for the Brownian and elastic stresses [12], whereas the second term accounts for the repulsive interaction in the same manner as in suspensions of interacting beads. Since the interaction is short range, it is sufficient to sum only over the beads of the chain together with the corresponding closest obstacles in the manner indicated in Eq. (8).

### 3.1. Numerical procedure and results

In this case, the actual calculations also involved nondimensional variables. The obstacle mesh size  $a$  was again used as the unit length, the unit time was  $\zeta \ell_0^2 / k_B T$  and the unit force  $k_B T / \ell_0$ . The choice of the parameters appearing in the set of Eqs. (5)–(7) was as follows. Since the ratio  $\ell_0/a$  must be significantly smaller than unity to allow fluctuation of the chain in the mesh of obstacles, the value 0.25 was adopted, the spring constant  $K = 100$  being used. This value determines the maximum allowable value of the time step  $\Delta t$ , which was set at  $4 \times 10^{-3}$ . In order to make the repulsive obstacle forces sufficiently stronger than Brownian forces (at the adopted  $\Delta t$  value), we let  $M = 25$ . Finally, we let  $s = 0.2$  (leaving a space of 0.6 for chain fluctuations) and  $q = 200$  in Eq. (5).

All runs were made with the chain initially located 'horizontally', i.e. along the shear direction, in the manner indicated in Fig. 13. The reason for such a choice is that fast flows should orient the 'tube of constraints' essentially horizontally; we thus saved simulation time in

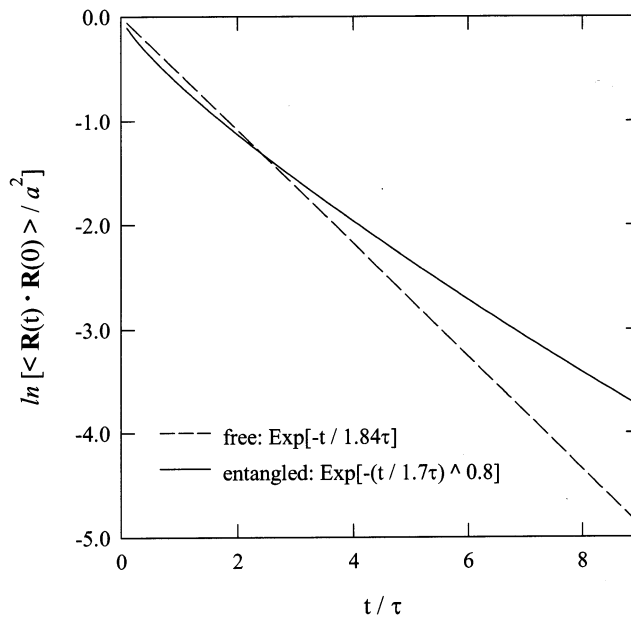


Fig. 12. Relaxation of the end-to-end vector correlation for a chain with  $N=3$ . While the free chain relaxes exponentially, the entangled one follows a stretched exponential.

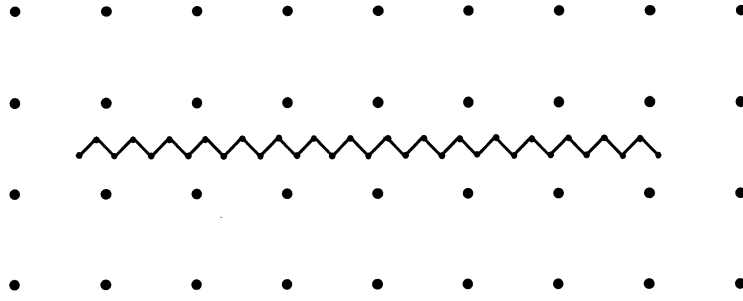


Fig. 13. Initial condition for the chain in the grid of obstacles. The chain soon relaxes the precise conformation.

this respect. Regarding ensemble averages at steady state, we actually exploited ergodicity and used time averages instead. In other words, we simply kept running with the same molecule for a sufficient period of time and sampled the stress periodically to calculate the averages.

Fig. 14 compares the first normal stress difference  $N_1$  contributed by a single chain at low and high shear rates. The abscissa in Fig. 14 is the deformation of the continuum, i.e.  $\dot{\gamma}t$ . The chain is rather long ( $N = 256$ ); hence, the nondimensional Rouse time is very large:  $\tau_{\text{chain}} = N^2 \cong 6.5 \times 10^4$ . Fig. 14 shows different behaviors of the chain at low and high shear rates. At relatively low shear rates (upper part of the figure), the ‘signal’ fluctuates more or less uniformly. Conversely, at high shear rates quasi-periodic, very large fluctuations emerge from the background ‘noise’ (lower part).

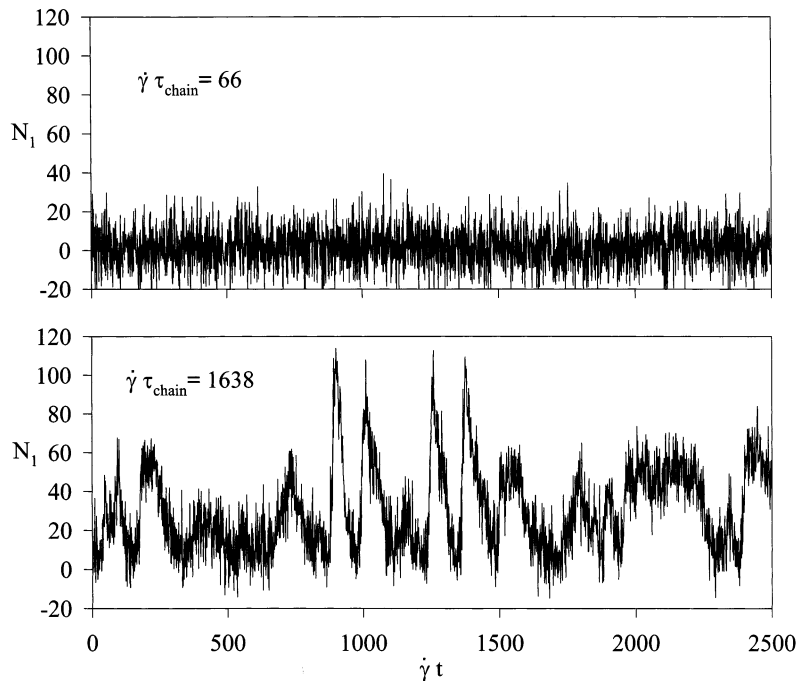


Fig. 14. Normal stress difference vs.  $\dot{\gamma}t$  for a long chain ( $N = 256$ ) in fast flows. At the larger value of  $\dot{\gamma}$  (lower part of the figure) the signal shows some significant structure.

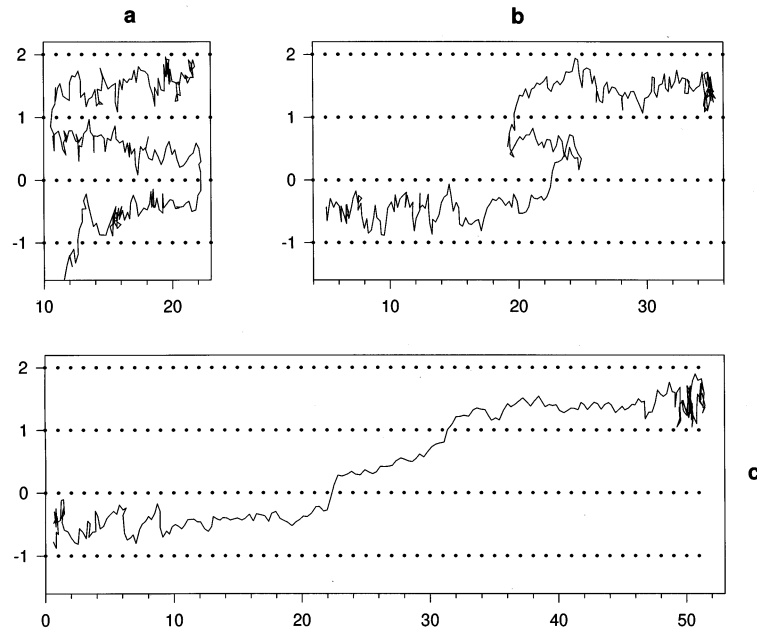


Fig. 15. Time evolution of chain conformation in the grid of obstacles (dots) at high shear rates. Chain ends fluctuate in the next layers and are convected away (a) thus generating a sigmoidal shape (b) which eventually becomes extremely stretched (c).

The peaks in Fig. 14 result from chain stretching, which occurs because of the mechanism depicted in Fig. 15. Indeed, computer animation of the chain dynamics reveals that the chain ends occasionally fluctuate out of the original ‘tube’ of obstacles into the next layer. The chain

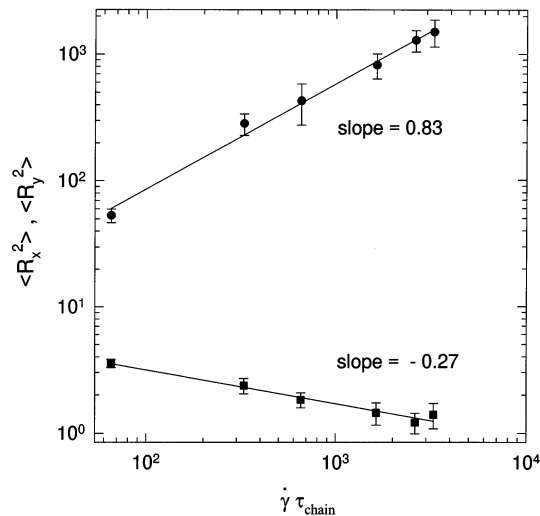


Fig. 16. Mean square size of the entangled chain ( $N = 256$ ) in the shear direction (upper curve) and in the gradient direction (lower curve). At the highest shear rate  $\langle R_y^2 \rangle$  is seen to approach unity (the obstacle mesh size), yet remains above it.

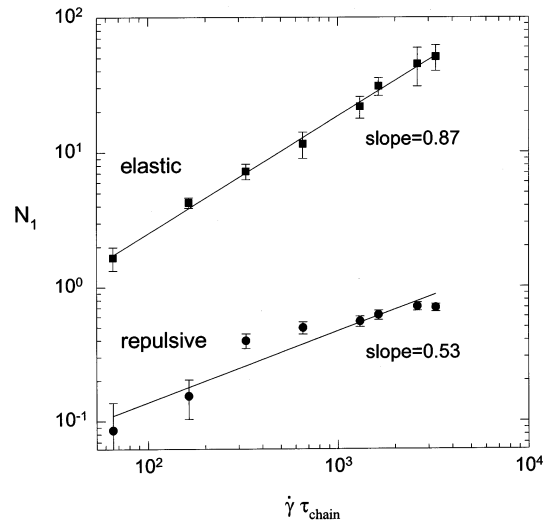


Fig. 17. The direct contribution to the stress tensor due to bead-obstacle repulsive interaction proves negligible with respect to that arising from chain elasticity.

then gets captured and stretched by the flowing material. The chain shape becomes sigmoidal for some time (Fig. 15a and b), then to quasi-horizontal (Fig. 15c) while the chain stretches. Eventually, the chain will relax, returning to the equilibrium length within a horizontal tube and the cycle can start again. It seems plausible that such a mechanism dominates the response in fast shear flows.

Average values are reported in Figs. 16–18. In particular, Fig. 16 shows the mean-square-size along both  $x$  and  $y$  for the  $N = 256$  chain as a function of the shear rate. As one might expect,

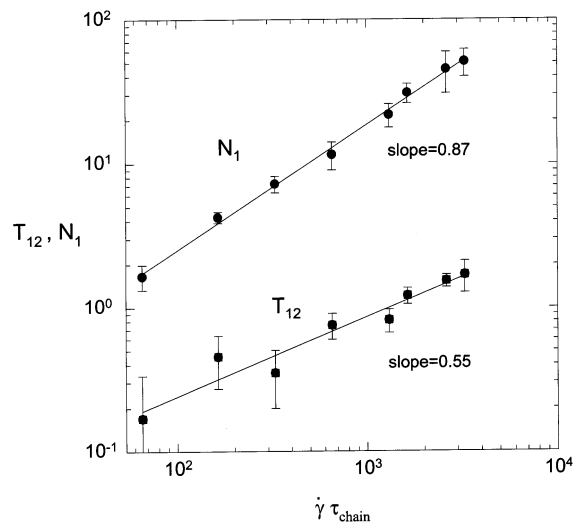


Fig. 18. Shear stress and normal stress difference vs.  $\dot{\gamma}$  at high shear rates. The simulation predicts a positive exponent of the power law for  $T_{12}$ .

the chain becomes more and more aligned in the flow direction with increasing shear rate. It should be noted however, that the size in the  $y$  direction always remains larger than 1 (the mesh size), thus revealing that on average the chain ends always lie in different layers.

Fig. 17 shows the values of the normal stress difference separately contributed by the repulsive and the elastic forces, thus demonstrating that the repulsive contribution is much smaller than the elastic one. Thus, it appears that the repulsive force introduced in order to preserve topology does not affect the stress directly. Of course the topology does affect the stress, as it greatly modifies polymer configurations with respect to the dilute case.

Finally, Fig. 18 reports the shear stress and the normal stress difference as a function of the shear rate. In the range explored, both quantities can be fitted with power laws having positive exponents. Regarding the shear stress, it so appears that chain stretching effects overcome chain orientation in the shear direction.

#### 4. Conclusions

Two-dimensional Brownian dynamics simulations of polymer chains constrained in a mesh of obstacles which move affinely with the applied flow were developed. A first, more rigorous model was developed with the purpose of isolating topological contributions—which only affect dynamics—from excluded volume contributions, which also affect equilibrium properties. That model, used only under quiescent conditions for reasons of computational efficiency, showed that chain diffusivity undergoes a rather slow transition to the entangled state. More precisely, the change from the  $-1$  to the  $-2$  power law of diffusivity vs. molecular weight seems to occur over a wide range of chain lengths, a feature which perhaps deserves further study. We also plan to explore other codes for the same model, which may enable us to investigate longer chains.

With a second model, where topology was enforced via excluded volume, the behaviour of entangled chains at high shear rates was investigated. A complex dynamical behaviour (a sort of tumbling) of the chains constrained by the obstacles was found. Fluctuations of the chain ends into the next layers between obstacles induced S-shaped configurations followed by substantial chain stretching. It appears that the stress tensor is dominated by these stretching events at high shear rates. A better understanding of such a complex dynamical behaviour might allow prediction of the shear rate and molecular weight dependencies of the frequency, duration and height of the stress peaks contributed by each chain and hence, the average response of the concentrated system. Work is also in progress in this direction.

#### Acknowledgements

This study was supported by the European Union through the EEC contract CHRX-CT93-0200. Thanks are due to S. Danese for carrying out some of the numerical calculations of the first model.

**References**

- [1] J.D. Ferry, *Viscoelastic Properties of Polymers*, Wiley, New York, 1980.
- [2] S.F. Edwards, The statistical mechanics of polymerized material, *Proc. Phys. Soc.* 92 (1967) 9.
- [3] P.G. de Gennes, Reptation of a polymer chain in the presence of fixed obstacles, *J. Chem. Phys.* 55 (2) (1971) 572.
- [4] M. Doi, S.F. Edwards, *The Theory of Polymer Dynamics*, Clarendon Press, Oxford, 1986.
- [5] M.E. Cates, T.C.B. McLeish, G. Marrucci, The rheology of entangled polymers at very high shear rates, *Europhys. Lett.* 21 (4) (1993) 451.
- [6] N.A. Spenley, M.E. Cates, Pipe models for entangled fluids under strong shear, *Macromolecules* 27 (1994) 3850.
- [7] S.F. Edwards, Statistical mechanics with topological constraints: I, *Proc. Phys. Soc.* 91 (1967) 513.
- [8] N. Saito, Y. Chen, Statistics of a random coil in presence of a point (two-dimensional case) or line (three-dimensional case) obstacle, *J. Chem. Phys.* 59 (1973) 3701.
- [9] J. Honerkamp, *Stochastic Dynamical Systems*, VCH, New York, 1993.
- [10] H.C. Öttinger, *Stochastic Processes in Polymeric Fluids*, Springer, Berlin, 1996.
- [11] J.S. Shaffer, Effects of chain topology on polymer dynamics: configurational relaxation, *J. Chem. Phys.* 103 (1995) 761.
- [12] R.B. Bird, C.F. Curtiss, R.C. Armstrong, O. Hassager, *Dynamics of polymeric liquids*, Vol. 2, *Kinetic Theory*, Wiley, New York, 1987.